Available online at www.sciencedirect.com
ScienceDirect
Geochimica et Cosmochimica Acta 75 (2011) 2529–2543
Geochimica et Cosmochimica Acta
www.elsevier.com/locate/gca

Seawater nutrient and carbonate ion concentrations recorded as P/Ca, Ba/Ca, and U/Ca in the deep-sea coral *Desmophyllum dianthus*

Eleni Anagnostou [a,*], Robert M. Sherrell [a,b], Alex Gagnon [c], Michele LaVigne [a,d], M. Paul Field [a], William F. McDonough [e]

[a] *Institute of Marine and Coastal Sciences, Rutgers University, New Brunswick, NJ 08901, USA*
[b] *Department of Earth and Planetary Sciences, Rutgers University, Piscataway, NJ 08854, USA*
[c] *Lawrence Berkeley National Lab, Berkley, CA 94720, USA*
[d] *University of California Davis, Bodega Marine Laboratory, Bodega Bay, CA 94923, USA*
[e] *Department of Geology, University of Maryland, College Park, MD 20742, USA*

Received 23 February 2010; accepted in revised form 14 February 2011; available online 21 February 2011

Abstract

As paleoceanographic archives, deep sea coral skeletons offer the potential for high temporal resolution and precise absolute dating, but have not been fully investigated for geochemical reconstructions of past ocean conditions. Here we assess the utility of skeletal P/Ca, Ba/Ca and U/Ca in the deep sea coral *D. dianthus* as proxies of dissolved phosphate (remineralized at shallow depths), dissolved barium (trace element with silicate-type distribution) and carbonate ion concentrations, respectively. Measurements of these proxies in globally distributed *D. dianthus* specimens show clear dependence on corresponding seawater properties. Linear regression fits of mean coral Element/Ca ratios against seawater properties yield the equations: P/Ca_{coral} (μmol/mol) = (0.6 ± 0.1) P/Ca_{sw}(μmol/mol) – (23 ± 18), $R^2 = 0.6$, $n = 16$ and Ba/Ca_{coral}(μmol/mol) = (1.4 ± 0.3) Ba/Ca_{sw}(μmol/mol) + (0 ± 2), $R^2 = 0.6$, $n = 17$; no significant relationship is observed between the residuals of each regression and seawater temperature, salinity, pressure, pH or carbonate ion concentrations, suggesting that these variables were not significant secondary dependencies of these proxies. Four *D. dianthus* specimens growing at locations with $\Omega_{arag} \leqslant 0.6$ displayed markedly depleted P/Ca compared to the regression based on the remaining samples, a behavior attributed to an undersaturation effect. These corals were excluded from the calibration. Coral U/Ca correlates with seawater carbonate ion: U/Ca_{coral}(μmol/mol) = (−0.016 ± 0.003) $[CO_3^{2-}]$ (μmol/kg) + (3.2 ± 0.3), $R^2 = 0.6$, $n = 17$. The residuals of the U/Ca calibration are not significantly related to temperature, salinity, or pressure. Scatter about the linear calibration lines is attributed to imperfect spatial-temporal matches between the selected globally distributed specimens and available water column chemical data, and potentially to unresolved additional effects. The uncertainties of these initial proxy calibration regressions predict that dissolved phosphate could be reconstructed to ±0.4 μmol/kg (for 1.3–1.9 μmol/kg phosphate), and dissolved Ba to ±19 nmol/kg (for 41–82 nmol/kg Ba_{sw}). Carbonate ion concentration derived from U/Ca has an uncertainty of ±31μmol/kg (for 60–120 μmol/kg CO_3^{2-}). The effect of microskeletal variability on P/Ca, Ba/Ca, and U/Ca was also assessed, with emphasis on centers of calcification, Fe–Mn phases, and external contaminants. Overall, the results show strong potential for reconstructing aspects of water mass mixing and biogeochemical processes in intermediate and deep waters using fossil deep-sea corals.

1. INTRODUCTION

Tropical corals are widely used in paleoceanographic reconstructions to provide high resolution records of

* Corresponding author. Address: Institute of Marine and Coastal Sciences, Rutgers University, 71 Dudley Road, New Brunswick, NJ 08901, USA. Tel.: +1 732 932 6555x252.
E-mail address: eleni@marine.rutgers.edu (E. Anagnostou).

0016-7037/$ - see front matter © 2011 Elsevier Ltd. All rights reserved.
doi:10.1016/j.gca.2011.02.019

climate variability. The absence of zooxanthellate corals below the surface layer of the ocean is a limitation that could be compensated by the presence of deep-sea corals, if suitable geochemical proxies in the skeletons of these organisms were developed. Azooxanthellate deep corals are globally distributed, and can be dated precisely with U–Th radiometric techniques. Fossil deep sea corals of appropriate age can thus be used to study the ocean's role in abrupt climate events including Heinrich events, the Younger Dryas, the Medieval Warm Period, and the Little Ice Age, if the range of useful proxies can be expanded.

The solitary coral *Desmophyllum dianthus* (*D. dianthus*) is an aragonitic scleractinian, azooxanthellate coral, with cosmopolitan geographic distribution, depth range of 35–2500 m (Cairns, 1994), and exceptional thermal tolerance of −1 °C to 28 °C (Stanley and Cairns, 1988). Because of its century-long life span and relatively large skeleton (~10 cm of vertical septal growth) (Cheng et al., 2000; Adkins et al., 2004), *D. dianthus* allows for both U/Th and radiocarbon dating (Cheng et al., 2000; Robinson et al., 2005) in addition to multi-proxy studies on a single specimen, providing the potential for subdecadal resolution of century scale windows into mesopelagic variability in the past (Adkins et al., 1998). There is great incentive, then, to develop new proxies that could provide high resolution information related to water mass mixing ratios and to the biogeochemical processes of nutrient supply and distribution, primary production, and biogenic particulate carbon flux to the intermediate and deep ocean.

Foraminiferal proxies currently used to reveal aspects of nutrient supply and utilization include $\delta^{13}C$, Cd/Ca (Keigwin and Boyle, 1989; Rosenthal et al., 1997), Ba/Ca (Lea and Boyle, 1990), and $\delta^{15}N$ (Altabet and Curry, 1989). In tropical corals these biogeochemical processes are explored using $\delta^{13}C$, Ba/Ca (Lea et al., 1989; Tudhope et al., 1996; Alibert and Kinsley, 2008), and Cd/Ca and P/Ca (Shen et al., 1987; LaVigne et al., 2010). A P/Ca proxy calibration was previously proposed for *D. dianthus* (Montagna et al., 2006), suggesting that P/Ca in the skeleton is ~7 times greater than P/Ca in ambient seawater. Questioning the validity of this outcome led to further research and resulted in the revised P/Ca calibration presented in this paper.

The deep sea coral *D. dianthus* also holds promise for reconstructing paleo-carbonate ion concentrations. Foraminiferal carbonate ion proxies, U/Ca in planktonics, and Zn/Ca and B/Ca in benthics (Russell et al., 2004; Marchitto et al., 2005; Yu and Elderfield, 2007), offer great promise but lack the high resolution and precise dating potential of *D. dianthus*. In tropical corals, the effect of carbonate ion concentration on uranium incorporation has been investigated but is difficult to distinguish against the stronger influences of temperature and other variables (Min et al., 1995; Shen and Dunbar, 1995). The limited temperature range of deep coral environments suggests that other influences on U/Ca variations, including potentially carbonate ion concentration, may emerge, but this potential has yet to be explored.

In this paper, we present evidence supporting three new proxy calibrations in the deep-sea coral *D. dianthus*: (1) a revised P/Ca proxy calibration for reconstructing seawater phosphate, (2) a Ba/Ca proxy for tracing variations in the silicate-type element Ba, and (3) a U/Ca proxy for carbonate ion concentration. The results constitute completion of the first steps required to greatly expand the potential utility of *D. dianthus* as a geochemical paleoceanographic archive. Further investigations will be required to fully quantify the effects of secondary environmental variables (temperature, salinity, pH, etc.) on the proposed proxies, through future field studies in which hydrographic parameters are well constrained, and through culturing experiments.

2. MATERIALS AND METHODS

2.1. Sample preparation and analytical approach

Samples were obtained from the National Museum of Natural History (Smithsonian Institution, Washington, DC) and from Dr. E. Sikes (Rutgers University, New Jersey, USA). The corals were treated with the ultrasonic-cleaning protocol of Cheng et al. (2000), and then septa were removed, cut longitudinally, mounted in epoxy and prepared as polished thick sections (300 μm) to ~1 μm roughness ensuring a flat surface for maintaining laser focus and signal stability. The thick sections were subsequently rinsed with isopropyl alcohol (99.9% purity) in an ultrasonic bath for several seconds and dried with a soft cloth. The sections were oriented along the growth axis, to enable sampling of the fibrous (acicular) aragonite portion of the septa, while visualizing the central band, septal exterior, and bioeroded features, all within the ~1 mm width of a typical septum.

The samples were ablated using a 193 nm ArF excimer laser (UP-193, New Wave Research Fremont, CA). Pure He was used as the ablation atmosphere (Eggins et al., 1998), and the output from the laser ablation cell was then mixed with additional Ar before injection into the central channel of the MS. The sample was ablated at a fluence of ~6–7 J/cm^2 and 15 Hz shot frequency. Gas blanks were measured initially for 45 s, while the laser beam was blocked by a shutter. The shutter was then opened, and the sample was ablated while the transient analyte signals were acquired for the ablation period.

Our sampling strategy was to ablate lines along the growth axis of the corals, integrating several years of growth, to obtain mean elemental composition for the specimen. Surface contamination, which in the case of our *D. dianthus* thick sections originated most probably from sample sectioning and polishing, was removed with preablation laser passes (Sinclair et al., 1998). Such contamination was expected to be restricted to the upper few microns since deep sea coral aragonite is dense and generally free of voids (^{43}Ca shows ~10% signal intensity variation along an ablation line). Therefore our approach was to perform preablation passes until averaged elemental ratios were reproducible among successive ablations of the same line (typically better than ±10%, see also Table A1). Typically we found that one ablation of ~6 μm depth was sufficient to remove surface contamination in coral thick sections, identified as a laser pass in which resultant data did not sat-

isfy the reproducibility requirements stated above. Ablation depth is estimated using a value of 1 μm per 10 shots, similar to other laser systems (Günther et al., 2000; Hathorne et al., 2003).

Analyses were carried out on an Element 2 SF–ICP–MS (ThermoFinnigan, Bremen, Germany) using a combination of magnet jumps and electrostatic peak scanning (E-scan). All elements were analyzed in medium resolution (MR = 4000 M/ΔM) to resolve molecular ion interferences on phosphorus (e.g. NO^+ and NOH^+) and on iron (e.g. ArO^+ and CaO^+), while acquiring time-resolved data in a near-simultaneous manner. The isotopes measured and the method parameters are listed in Table 1. For the selected laser and ICP conditions (Tables 1 and 2), elemental ratio precision of coral analyses in thick sections was typically <±3% (1SD) for Ba/Ca, <±5% (1SD) for U/Ca, and <±6% (1SD) for P/Ca for 3–4 replicate ablations of the same line, integrated to obtain mean El/Ca for each ablation pass. The length of ablated line varied depending on sample from 0.4 to 4.0 mm. The gas blank, in counts per second (cps), as a fraction of mean coral signal intensity (cps), was <4% for P, <1% for Ba, and not detectable for U, while Ca blank was <1% and Fe and Mn blanks, depending on the sample, were typically <20%.

Table 1
SF–ICP–MS acquisition parameters.

Isotope	Sample time (s)	Detection mode
^{11}B	0.010	Counting/analog
^{25}Mg	0.003	Counting/analog
^{31}P	0.010	Counting/analog
^{43}Ca	0.003	Analog
^{55}Mn	0.003	Counting/analog
^{56}Fe	0.003	Counting/analog
^{136}Ba	0.003	Counting/analog
^{238}U	0.003	Counting/analog
Resolution m/Δm: 4000		
Mass window: 40%		
Search window: 10%		
Integration window: 15%		
Samples per peak: 40		
Scan type: E-scan		
Total duty cycle: 73%		

Table 2
SF–ICP–MS and laser ablation parameters.

SF–ICP–MS	Element 2	ThermoFinnigan, Bremen, Germany
RF power		1250 W
Sample gas (Ar)		0.8–0.9 L min^{-1}
Coolant gas flow		16 L min^{-1}
Auxiliary gas flow		1.06 L min^{-1}
Sampler, skimmer cones		Ni
Laser ablation	UP193HE	New Wave Research, CA, USA
Pulse width		20 ns
Energy		0.5–0.6 mJ
Fluence		6–7 J/cm^{-2}
Laser repetition rate		15 Hz
Laser spot size		80–100 μm
Scan speed		15–25 μm/s^{-1}
Carrier gas (He)		0.75 L min^{-1}

Standardization was achieved by bracketing each coral ablation line with NIST 612 glass standard analyses (~2 mm long scan), interpolating a linear mass-response gradient between standards (Eggins and Shelley, 2002; Hathorne et al., 2008). To correct for variations in ablation yield and instrumental drift, element signals were normalized to Ca as the internal standard (Longerich et al., 1996b; Hathorne et al., 2003). We used spreadsheet software for offline data reduction, which involved gas-blank subtraction, normalization to ^{43}Ca, removal of signal spikes (rare: when present, El/Ca was at least a factor of 2 higher than the maximum El/Ca ratios within the rest of the ablation line) that probably represented contaminant particles entering the plasma (Sinclair et al., 1998), and finally, standardization. The NIST 612 standard is considered homogeneous for Ba, Ca, P and U (Eggins and Shelley, 2002), therefore published elemental concentrations were used (Ba: 39.7 ppm and certified U: 37.4 ppm; Reed, 1992; Jochum et al., 2005, Ca: 84690 ppm; Eggins, 2003, P: 39.9 ppm; LaVigne et al., 2008). The lack of appropriate carbonate standards for this study led to the use of the non-matrix matched glass standard. Any matrix dependent elemental fractionation is, however, minimized for most elements when using 193 nm lasers, including Ba and U (Longerich et al., 1996a; Guillong et al., 2003; Hathorne et al., 2008). For P/Ca measurements, it has been shown that analyses using solution SF–ICP–MS agree with 193 nm laser ablation SF–ICP–MS measurements in tropical corals for specific operational conditions (LaVigne et al., 2008). To minimize mass load induced matrix effects and laser induced fractionations, we selected laser and plasma conditions similar to those of LaVigne et al. (2008) (Table 2).

A sub-set of three corals (47413, 83583, 82065) was analyzed using colorimetric techniques (Koroleff, 1983) to quantify the contribution of inorganic phosphate to the total P content of the coral. Subsamples of the septa were removed and crushed, then dissolved in 0.8 N hydrochloric acid (trace metal grade). For the purpose of color development, the final solution was diluted in distilled water to a working pH of ~1 (Anagnostou and Sherrell, 2008). This method quantifies the soluble reactive phosphorus fraction in solution, and includes monophosphates but excludes organic phosphorus compounds and non-reactive inorganic phosphates including pyro- and polyphosphates.

2.2. Data analysis

Deep-sea coral specimens were collected at locations characterized by a range of seawater properties. Hydrographic data were varyingly well constrained depending on station locations from the current global ocean database (WOCE, GEOSECS, and CLIVAR programs) as well as from other published data. When necessary due to geographic coverage of water column data, seawater properties

were extrapolated along isopycnals from available hydrographic stations to coral collection sites (Tables A1 and A2). To quantify the uncertainty in seawater concentrations from potential spatial and temporal mismatch between the coral collection and the hydrographic station selected, we compiled all available data from locations within a range of latitude (5°) and longitude (35°) and within 27 years of the selected primary hydrographic station for each coral specimen (listed in Table A2). None of our corals has been radiometrically dated, although they are thought to have been collected alive since we observed residual dried tissue on all corals but 94069 and 48739.

The calibration slopes, regression coefficients (R^2), *y*-intercepts and associated errors were calculated using Type-2 geometric mean linear regression, otherwise known as reduced major axis (Ricker, 1973; Bevington and Robinson, 1992), as modified for Matlab by E. T. Peltzer (for details, see http://www.mbari.org/staff/etp3/regress.htm). The error envelopes were computed using the Matlab toolbox CurveFit (2009) for linear regression.

3. MICROSKELETAL VARIABILITY

Before establishing a consistent procedure that generated reproducible elemental ratios, different structural features were analyzed in the deep sea coral *D. dianthus*. The phases examined included the fibrous aragonite, centers of calcification (COCs), Fe–Mn phases, and the exterior of the septa. We developed data acceptance criteria for the elements of interest and established best practices for measuring our geochemical proxies in *D. dianthus* with laser ablation.

3.1. Effects of Fe–Mn phases on intra-skeletal elemental ratio variations

It has been reported that Mn-rich phases can contain trace element contaminants, compromising elemental ratio reconstructions in foraminifera (Pena et al., 2008). In corals, such phases may be Fe–Mn oxide and hydroxide inclusions, contaminant particles (e.g. particulate phosphorus), Fe biominerals (Konhauser, 1997), or carbonate material precipitated during conditions of high particulate organic matter flux and surface sediment suboxia, leading to enrichment in Fe, Mn, and P in the local benthic nepheloid layer (Sherwood et al., 1987).

To investigate potential contamination by Fe–Mn phases, lines were ablated on the surface of coral septa, cut and cleaned as described above for thick sections (Fig. 1). We observed apparent contaminant phases evidenced by local peaks in Fe/Ca and Mn/Ca, associated with P/Ca signals elevated by at least a factor of 2 (Fig. 2), which were typically removed with subsequent ablations of the same area, suggesting that their dimensions in the ablation z-axis were a few 10 s of μm. Especially for corals recovered from suboxic waters, like *D. dianthus* specimen 84818 (12 μmol/kg oxygen; Table A2), proximity to sediment-source dissolved Mn^{2+} could lead to precipitation of Mn carbonates, with elemental composition distinct from that of the carbonate hosts (Pena et al., 2005).

Taking advantage of the multi-element analytical approach in our study, we suggest that when Fe/Ca, Mn/Ca, and P/Ca co-vary, and there is a $\geqslant$2-fold increase in Mn/Ca and Fe/Ca compared to the mean along the rest of a coral ablation line, discrete Fe–Mn phases enriched in P may be present. These phases did not show anomalous enrichment in Ba or U (Fig. 2). However, ablation of interior septal aragonite accessible in thick sections, with preablation, allowed us to avoid these septal surface phases, such that no P/Ca data needed to be edited from our raw data set for association with high Mn or Fe. This evidence justified use of septal thick sections for the remainder of the study.

3.2. Variations in the central band and centers of calcification

Two discrete structures (Fig. 1) described in scleractinian coral skeletons are the centers of calcification (COCs)

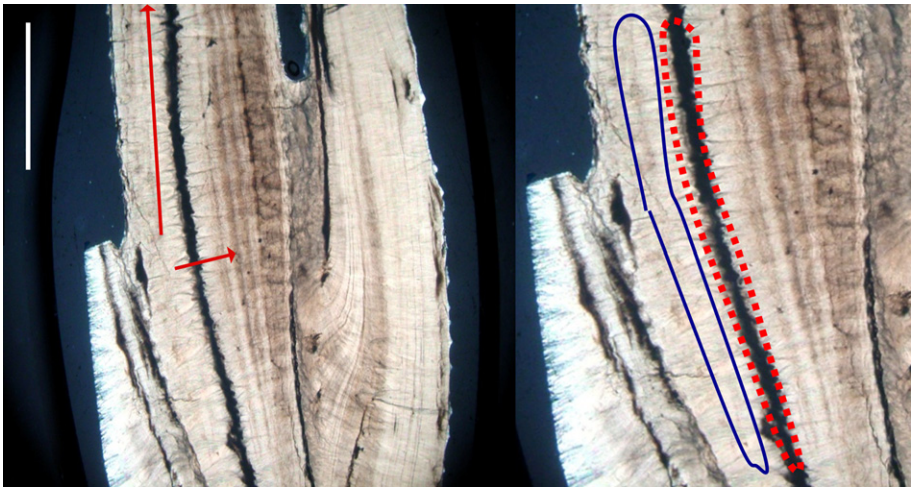

Fig. 1. Transmitted light image of an S1 septum and two neighboring S2 septa of a *D. dianthus* coral showing the internal banding pattern (magnified image on the right). Central band (with COCs) in dotted outline shows as dark color, in contrast to the region of fibrous aragonite crystals (solid outline). Lines with arrows on left image are examples of laser ablation tracks analyzed. Ablation across the central band is used to explore elemental anomalies in that region. Scale bar in upper left represents 1 mm.

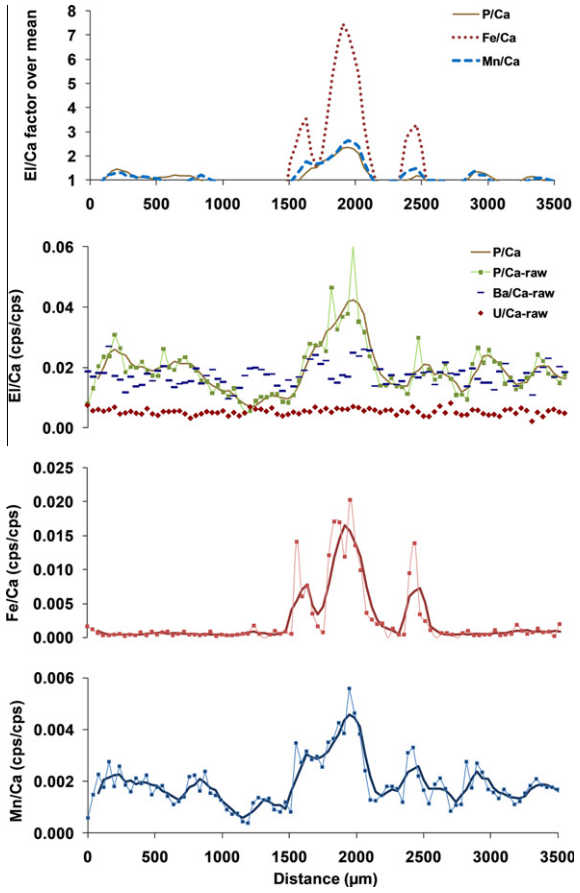

Fig. 2. Elemental ratios for ablation of a 3.5 mm line along the exterior of a *D. dianthus* septum. This coral has a distinct Fe–Mn phase that is associated with factor of ~3 increase in P/Ca ratios at the center of ablation line. Symbols and thin lines represent raw data, while bold lines represent 4-point moving averages. The top panel shows Element/Ca normalized to the mean ratio for portions of the ablation line outside the central Fe–Mn–P peak, to emphasize the relative magnitude of the compositional anomaly. For reference, U/Ca and Ba/Ca raw ratios are also shown.

located in the central band, and clusters of fibrous crystals radiating out from the centers (Ogilvie, 1896; Bryan and Hill, 1941). The COCs are morphologically (Constantz, 1986; Cohen et al., 2001) and compositionally (e.g. Adkins et al., 2003; Cuif et al., 2003; Meibom et al., 2006) distinct from the surrounding aragonite. We attempted to map the variability of elemental ratios across the central band of coral 62309 by drilling 100 μm spots on either side of and directly focused on central band material, for 4 regions along the central band of a single septum (Fig. 3). The behavior of Mg/Ca and U/Ca in the central band was in general agreement with the findings of other studies, displaying enrichment in Mg/Ca and depletion in U/Ca (Sinclair et al., 2006; Gagnon et al., 2007). Although no P/Ca anomalies in central band material were resolvable against P/Ca ratios in non-COC portions of the ablated areas, it was obvious that P/Ca was more variable in the central band than in fibrous aragonite regions (error bars in Fig. 3). Additionally, Ba/Ca was largely invariant across the central band in contrast to recent observations in tropical corals and artificially precipitated granular aragonite aggregates (Holcomb et al., 2009). Our results demonstrate clearly the importance of avoiding the central band if precise U/Ca and P/Ca measurements are to be made. The criterion for data removal due to inadvertent ablation of COCs in our study was that the data in the anomalous region displayed Mg/Ca >2-fold higher and U/Ca ⩾2-fold lower than the mean of the remaining ablation line. Editing for the presence of COCs was required only for coral specimens 19168 and 84820.

3.3. Ablation of thick sections versus exterior of septa

In preliminary experiments, we attempted to determine accurate and consistent values for the proxy element ratios by ablating the exterior surfaces of septa, seeing the advantage of the simplified sample preparation and expected avoidance of the central band by limiting ablation penetration depth, following the methods of Montagna et al. (2006). We observed that this approach requires more extensive and thus deeper preablation (>20 μm compared to <10 μm for thick sections) to remove anomalous surface phases.

The nature of these phases on the surfaces of septa is likely complex and variable. We separate them into two categories; phases precipitated or included during the coral polyp lifetime, and phases generated post mortem. Deep sea corals are frequently located in waters undersaturated with respect to aragonite, but the tissue layer protects the skeleton against dissolution. In times of environmental stress, however, corals may retract the polyp exposing the exterior of the corallite to corrosive waters and therefore to erosion and dissolution (Lazier et al., 1999), resulting in anomalous minor element ratios caused by differential leaching (Hendy et al., 2007). Endolithic borings could also be filled with aragonitic or calcitic cements (Nothdurft et al., 2007; Cusack et al., 2008). Post-mortem, dissolution, boring, and infilling may continue, and early marine aragonite cement may precipitate on the skeletal surface, altering the values of important geochemical proxies. Such cements can be avoided by assuring that sampling does not intersect the margins (e.g. external areas of septa and the coral wall) or surfaces of internal structures (e.g. central band material and borings) (Nothdurft et al., 2007; Perrin and Smith, 2007).

Preablation of the exterior of septa does not guarantee the removal of altered material at the surface of the coral. For example, following preablation, the analytical ablation lines on the exterior surfaces frequently intersected regions of elevated Mg/Ca and decreased U/Ca, indicating the presence of COCs near the septal surface (e.g. Fig. 1), often not visible with light microscopy. We concluded that altered phases on the septal surface can be too irregular in thickness and the presence of COCs too difficult to confirm, to make exterior ablation a viable method for obtaining precise and representative elemental data.

Given these potential problems with ablation of the exterior of septa, we analyzed interior septal aragonite in thick sections. Ablation lines were laid out within the

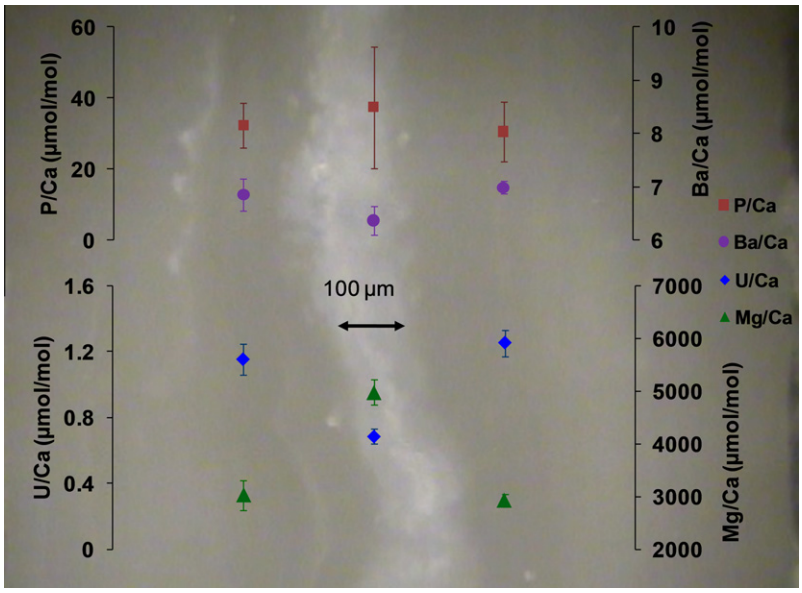

Fig. 3. Results of ablation of 100 µm spots within centers of calcification (COCs; white central band under reflected light) and in the fibrous part of coral 62309, outside of the COCs, shown against a reflected light image of thick section of septum. In the areas where COCs are present, Mg/Ca is elevated and U/Ca is decreased. The Ba/Ca is nearly invariant while P/Ca is highly variable within COCs. Error bars represent SD of the mean of 4 spots drilled at different points along each side of and within the central band. Data points are positioned relative to their respective scale bars, and do not reflect the positions of the ablation spots on the sample pictured.

Table 3
Examples of P/Ca, Ba/Ca, and U/Ca means from different ablation lines on the same and different septa. Uncertainties are SD among replicates of the same ablation line.

	P/Ca ± 1SD	Ba/Ca ± 1SD	U/Ca ± 1SD	Replicates
Coral 19249: 1.5–2 mm lines at tips of different septa				
Line 1 (µmol/mol)	118 ± 7	8.1 ± 0.8	2.1 ± 0.2	$n = 3$
Line 2 (µmol/mol)	118 ± 9	7.7 ± 0.3	2.0 ± 0.3	$n = 3$
Coral 62309: 4 mm parallel lines on S1 septum				
Line 1 (µmol/mol)	27	8.4	1.5	$n = 1$
Line 2 (µmol/mol)	22 ± 3	8.3 ± 0.4	1.4 ± 0.1	$n = 3$
Coral 94069: lines on different corals from the same location				
Coral 1 (µmol/mol)	65 ± 7	7.7 ± 0.4	1.65 ± 0.04	$n = 6$ (2 lines)
Coral 2 (µmol/mol)	61 ± 3	7.7 ± 0.2	1.76 ± 0.07	$n = 6$ (2 lines)

fibrous aragonite regions of the polished sections, away from central bands and the exterior of the septa, and along the coral growth axis. The resultant mean elemental ratios were highly reproducible in different areas of the fibrous regions of a septum, and in neighboring septa of the same individual (Table 3).

4. RESULTS AND DISCUSSION

4.1. The P/Ca nutrient proxy

To generate a global calibration of P/Ca against dissolved phosphate, we analyzed twenty corals from a number of geographic locations (Fig. 4) and depths, spanning nearly the full oceanic range of seawater phosphate (~0.5–3.0 µmol/kg). Among all hydrographic variables considered, coral P/Ca is most strongly correlated with dissolved phosphate, evidenced by regression against hydrographic data from nearby stations (Fig. 5a). The resultant slope was 0.6 ± 0.1 ($R^2 = 0.6$), and the y-intercept of −23 µmol/mol is indistinguishable from zero within the regression error envelope (Fig. 5a). Four samples were excluded from the calibration regression, for reasons stated below.

Our measured P/Ca linear regression slope of 0.6 differs markedly from the slope of ~7 measured in a previous calibration of P/Ca in the same species (Montagna et al., 2006). We suspect the discrepancy between our regression slope and that of Montagna et al. (2006) is a product of sampling approach. The authors acquired data by ablating the exterior of the septa, rather than thick sections, preceded only by a peroxide cleaning step and ~11 µm depth

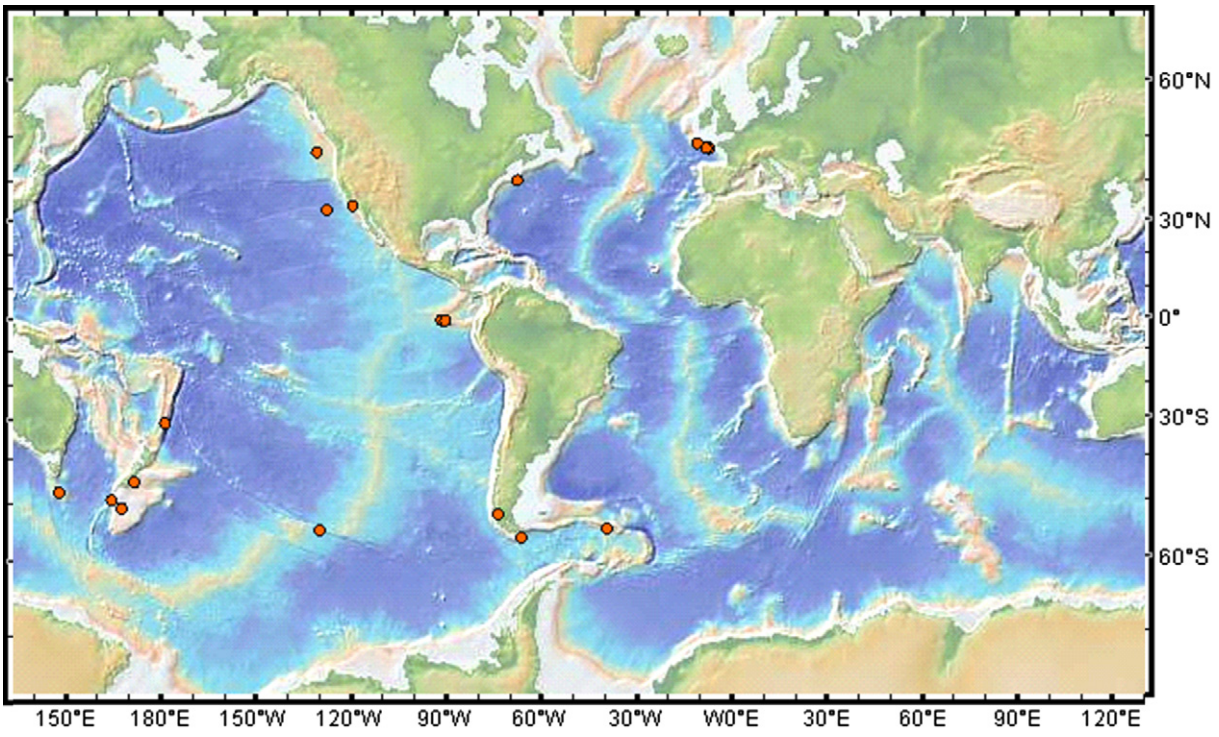

Fig. 4. Locations of *D. dianthus* corals (closed circles) used to generate proxy calibrations (GeoMap).

of preablation (assuming average laser ablation of 0.1 μm per shot, see Methods above). As described above, however, ablation of the exterior of septa requires more vigorous preablations to remove diagenetically altered material, Fe-Mn phases and other contaminants.

Although a useful test would be to analyze the same corals for Fe, we suspect that the strong co-variation that Montagna et al. (2006) observed between Mn/Ca and P/Ca in *D. dianthus* ($R^2 \sim 0.5$, up to 0.8 along some ablation paths) is an indication of presence of Fe–Mn phases and co-occurring P. We only saw this correlation in corals with anomalous Fe–Mn areas associated with high P, during ablations of the exterior of septa (Fig. 2). We propose that the 0.6 slope of our P/Ca proxy calibration represents more closely the composition of the uncontaminated fibrous aragonite, and that this material is only analytically accessible in *D. dianthus*, within practical limitations, by microsampling techniques on septal thick sections.

To investigate the sources of scatter in the P/Ca calibration, we tested the correlation between linear regression residuals and candidate secondary variables. For the corals used in the calibration we found no significant correlation between P/Ca residuals and temperature, salinity, pressure, pH or carbonate ion (all $R^2 < 0.3$). Since many hydrographic parameters in seawater co-vary, however, (e.g. seawater phosphate correlated with pH) this analysis of regression residuals needs verification through culture studies in which environmental variables can be isolated. Therefore dependence of P/Ca on both seawater phosphate and other variables, while not specifically observed in this study, could contribute to the scatter in the P/Ca-regression.

The mechanism(s) of P incorporation in corals remain poorly understood; hence the calibration we present is fundamentally empirical. In tropical coral skeletons, P has been shown to be dominantly intra-crystalline in nature, meaning it is distributed in or between individual aragonite crystals (LaVigne et al., 2008). Because the *D. dianthus* coral is less porous than tropical corals, we assume that after preablation of thick sections, and accepting data that are reproducible with depth of ablation, our analyzed P/Ca in *D. dianthus* is also dominantly intra-crystalline.

Both inorganic and organic phosphorus are thought to be present in coral aragonite (Dodge et al., 1984; Shotyk et al., 1995; LaVigne et al., 2008). In support to this hypothesis, our preliminary soluble reactive phosphorus (SRP; Koroleff, 1983) analyses performed on three corals yielded inorganic phosphorus concentrations at <10% of the total coral phosphorus content. Intra-crystalline inorganic phosphorus could be the result of ionic substitution within the coral aragonite or inclusion of discrete particulate phases like hydroxylapatite (Macintyre et al., 2000) and iron-phosphates. Although we cannot exclude the possibility of hydroxylapatite present in *D. dianthus* skeleton (though it should dissolve and be analyzed as SRP), we can refute the presence of iron-phosphate, because P/Ca is at least an order of magnitude higher than Fe/Ca in our corals, whereas Fe phosphates have a typical P/Fe ratio <0.12–0.23 (Feely et al., 1994).

Similarly to tropical corals, deep sea scleractinian corals contain up to 2.5% organic material (Cuif and Dauphin, 2004). Among the P rich organic material potentially present within the coral skeleton are lipids, DNA remnants and enzymes like alkaline phosphatase (Goreau et al., 1971).

Recently, Farré et al. (2010) suggested that lipids are an important component of organic matter in the skeleton of deep sea scleractinia, dominated by phospholipids. To our knowledge, there is no available quantification of total lipids in the skeleton of deep sea scleractinian corals. Performing a calculation similar to that in LaVigne et al. (2008), assuming up to 0.03% lipids per total *D. dianthus* skeletal material (Isa and Okazaki, 1987), and an average phospholipid molecular weight of 800, phospholipids in *D. dianthus* could contribute up to 39 μmol P per mol Ca. This concentration is within the lower range of our corals, suggesting that phospholipids may contribute a significant portion of total skeletal P. We need specialized studies to further examine the nature of phosphorus in coral skeleton including synchrotron-XRF and NMR approaches. Despite the apparent organic nature of coral P/Ca, our results indicate strongly that skeletal P concentrations are driven by variations in seawater inorganic phosphorus.

We also examined the possible effect of sample location on the scatter in the P/Ca calibration line. The coral specimens used in this study were collected from the Southern Ocean (poleward of 45°S), the N. Atlantic, the N. Pacific, and Pacific upwelling regions (Gulf of Alaska, California Coast, and Galapagos). We did not observe any location-related bias in the P/Ca values, with the exception of the four corals that were collected from upwelling regions, at depths where ambient waters are undersaturated with respect to aragonite ($\Omega_{arag} \leqslant 0.6$). The P/Ca values for these corals deviated markedly below the calibration regression defined by the remaining points and were not included in the regression (square symbols in Fig. 5a). Although the regression residuals excluding the four outlier points do not correlate with any ambient seawater parameters, when the upwelling corals are included in the sample set, the regression residuals do show an overall correlation with pH ($R^2 = 0.4$).

We suspect that corals living in seawater that is undersaturated with respect to aragonite are affected indirectly by bulk seawater pH. Undersaturation can drive slower net calcification rates, as observed for $\Omega < 0.8$ in tropical corals (Ries et al., 2010), due to the metabolic cost of achieving required levels of calcifying fluid supersaturation (Cohen et al., 2009). The mechanisms by which growth rate might affect P/Ca are not understood. Predictions and hypotheses are hindered at this point as the mechanism of P incorporation is unknown; models for elemental incorporation in non-biogenic carbonate are not directly comparable. Future studies in cultured corals could separately test the effect of aragonite undersaturation on coral P/Ca, especially for *D. dianthus*, in an effort to explain the observed offset in this study.

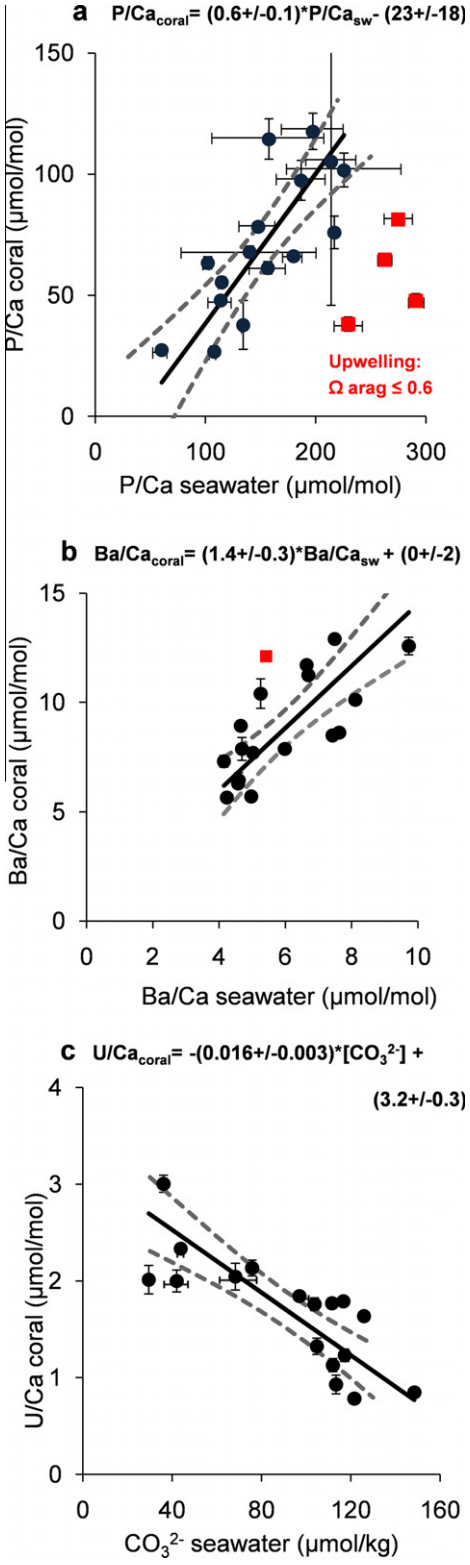

Fig. 5. Calibrations of P/Ca, Ba/Ca, and U/Ca proxies in *D. dianthus* against seawater compositional variables. Uncertainties in equations represent 1SD, and the error envelope (dotted lines) is calculated from the 95% confidence interval. Error bars in *y*-axis represent SD of replicate ablation lines on single and/or neighboring septa. For symbols without error bars, error is smaller than symbol or single ablation lines were analyzed (Table A1). Error bars in *x*-axis represent uncertainty (1SD) in relevant hydrographic data. Closed squares are outliers not used in the calibration regressions (see text).

4.2. The Ba/Ca nutrient-type proxy

The Ba/Ca ratios for 18 specimens of *D. dianthus*, plotted against available ambient Ba/Ca_{SW} data, yield a proxy calibration over a wide range of Ba concentrations, with small error bars and a y-intercept near zero (Fig. 5b). This is the first systematic calibration of the Ba/Ca proxy in a deep-sea coral. The *D. dianthus* Ba/Ca ratios are similar to those previously reported for the same species (Montagna et al., 2006), and the linear regression slope is 1.4 ± 0.3 ($R^2 = 0.6$), comparable to that determined previously for tropical corals and inorganic experiments for relevant temperatures (Lea et al., 1989; Dietzel et al., 2004). Of the corals analyzed, specimen 48470, located off the northern region of the Bay of Biscay, was located furthest away from a station with available Ba_{sw}, and the isopycnal approach we employed for deriving local Ba_{sw} thus carries more uncertainty. Indeed this sample plotted as a notable outlier in the regression, and was thus excluded from the calibration (square symbol, Fig. 5b).

The mechanism by which barium is incorporated into biogenic carbonate has been suggested to involve ionic substitution for Ca^{2+}, forming orthorhombic $BaCO_3$ (witherite) (Speer, 1983; Dietzel et al., 2004). We expected that Ba/Ca in *D. dianthus* would have some degree of temperature dependence based on the work of Lea et al. (1989). Plotting the Ba/Ca calibration residuals against corresponding *in situ* temperature, however, did not reveal a significant correlation ($R^2 = 0.1$). In support of this observation, Dietzel et al. (2004) reported <10% variation in average distribution coefficient of Ba/Ca for inorganic aragonite precipitated over a temperature range of 10–19 °C. Additionally, if we use the equation suggested by Gaetani and Cohen (2006) for the dependence of Ba/Ca on temperature ($\ln Ba/Ca = 2507/T - 5.9$), the range in Ba/Ca concentration describes a variation of ±9.7% (SD) about the mean coral Ba/Ca for the range of ambient temperatures for our corals (2–11 °C), which is small compared to the dependence of coral Ba/Ca on seawater Ba for this sample set, and is comparable to the 2SD reproducibility of the Ba/Ca measurements for *D. dianthus* coral sections (Table A1). It would be informative to compare our coral Ba/Ca with inorganic aragonite precipitation experiments carried out at appropriately low temperatures, but no such study has been published, hence we suggest that the temperature dependence of Ba/Ca is relatively insignificant compared to Ba-driven variations for deep sea coral aragonite precipitated at temperatures below 15 °C. Our regression of the primary calibration offsets against ambient temperature seems to suggest that indeed we are not able to discern any temperature dependence in our data set. Similarly, we investigated the dependence of Ba/Ca regression residuals on salinity, potential pressure (McCorkle et al., 1995), pH, and carbonate ion, but none was observed ($R^2 < 0.03$ in all cases). Finally, there was no consistently unique behavior for corals from upwelling regimes as was found for the P/Ca calibration.

The Ba/Ca ratio therefore appears to be a relatively uncomplicated proxy for dissolved barium. The scatter around the calibration line is suspected to result primarily from the uncertainty in hydrographic data for Ba_{sw}, but may also be affected by biological, growth rate, or regional effects that we were not able to identify or quantify in this calibration work.

4.3. The U/Ca carbonate ion concentration proxy

Coral U/Ca (μmol/mol) is most strongly correlated with ambient seawater carbonate ion concentration (μmol/kg), among the hydrographic variables tested (temperature, salinity, pressure, pH). This correlation is strongly negative with a slope of -0.016 ± 0.003 and y-intercept of 3.2 ± 0.3 μmol/mol (Fig 5c, $R^2 = 0.6$, $n = 17$). Carbonate ion concentrations were calculated from other reported carbonate system parameters using CO_2 sys.exe (Ver. 1.05; Lewis and Wallace, 1998; K_1 and K_2 were selected according to Mehrbach et al. (1973) refit by Dickson and Millero (1987)). The temperature, salinity, and pressure dependence of U/Ca was found to be negligible in *D. dianthus*, evaluated as above by plotting the residuals of individual samples in the carbonate ion linear regression against ambient hydrographic properties ($R^2 < 0.2$ in each case).

Since the aqueous chemistry of uranium is influenced by the carbonate ion, which forms complexes with the uranyl ion (UO_2^{2+}) (Langmuir, 1978), variations of U/Ca in tropical corals are suspected to be related to changes in seawater carbonate ion, but U/Ca is demonstrably correlated with temperature, the dominant influence (Min et al., 1995; Shen and Dunbar, 1995). In ooid formations, U content has also been shown to be inversely related to carbonate ion (Chung and Swart, 1990). Our results showed that *D. dianthus* U/Ca declined by ~58% for a 100 μmol/kg increase in carbonate ion, comparable to the 32% mean decline for the same carbonate ion increase observed in planktonic foraminifera cultures (Russell et al., 2004) but offset to higher U/Ca ratios in *D. dianthus*. This offset is expected since the ionic radius of UO_2^{2+} is larger than Ca^{2+} (Kitano and Oomori, 1971), and therefore the aragonite lattice with its orthorhombic structure and non-planar CO_3^{2-} group would allow more freedom for large ion substitutions than would calcite (De Villiers, 1971).

The scatter in our U/Ca carbonate ion calibration could be attributed to a number of factors, similar to those discussed for the P and Ba proxies; diagenesis and sample heterogeneity are not expected to have a major influence on the U/Ca calibration based on the sampling strategy followed. Further studies are needed however to fully quantify potential dependence of coral U/Ca on other hydrographic variables, e.g. temperature, which could cause an uncertainty in this calibration, although our hydrographic data did not indicate such an effect. The age of the analyzed corals is somewhat uncertain, adding potential error in the hydrographic properties assumed to be characteristic of ambient seawater conditions when the corals grew.

According to physicochemical models of coral calcification, aragonite is precipitated from modified seawater within an extracellular calcifying compartment, where carbonate ion concentration is actively elevated above ambient concentrations, facilitating crystal nucleation and growth (Al-Horani et al., 2003; Holcomb et al., 2009). Nevertheless, calcification processes (e.g. calcification rate) could be sensitive to variations in the saturation state of the external environment (Langdon et al., 2000; Cohen and McConnaughey,

2003; Ries et al., 2010), with implications for elemental incorporation, U speciation, U adsorptive efficiency, and ultimately coral U/Ca ratios. Potential routes by which carbonate ion could affect U/Ca incorporation in the coral aragonite are related to: (1) aqueous uranium speciation and diffusion, (2) subsequent adsorption and desorption, (3) ligand exchange reactions and rearrangement of ligand coordination, and (4) processes within the solid (e.g. solid diffusion and coordination changes; Russell et al., 2004 and references therein). The inverse relationship between coral U/Ca and carbonate ion could be a net result of several factors.

One of the processes affecting U/Ca in corals could be inhibition of adsorption of uranyl complexes on mineral and organic phases by high carbonate ion concentration because of competition for anion adsorption sites (Langmuir, 1978; Barnett et al., 2000). Additionally, assuming that *D. dianthus* calcification rates increase with higher carbonate ion concentrations similarly to tropical corals (Kleypas et al., 1999; Schneider and Erez, 2006), the U/Ca calibration implies that higher calcification rates suppress U incorporation. Coral studies and inorganic aragonite precipitation experiments suggest that tris-carbonated uranyl species are the dominant U form in aragonite (Swart and Hubbard, 1982; Reeder et al., 2000). The precipitation studies of Reeder et al. (2000), however, were conducted at $\Omega_{arag} = 15–28$ and pH > 8, not realistic conditions for a coral environment. The calcite precipitation experiments at lower pH (Reeder et al., 2001), where mono- and bi-carbonate uranyl complexes were also observed, could be more suitable for revealing the uranyl complex structure within the coral skeleton. If coral aragonite incorporates these uranyl complexes, the increasing coral U/Ca at lower carbonate ion concentrations in our study could imply the additional incorporation of mono and bi-carbonate uranyl complexes whose abundance increases at lower pH. Therefore, while the mechanisms may be complex and multiple, our result for *D. dianthus* is a simple and empirical anticorrelation between U/Ca and bulk seawater carbonate ion concentration. As a next step, inorganic aragonite precipitation experiments should be carried out to evaluate the carbonate ion effect on U/Ca ratios independent of vital effects and therefore to test the applicability of this proxy to paleoreconstructions.

5. CONCLUSIONS

In this work, P/Ca in the deep-sea coral *D. dianthus* is shown to be a linear function of seawater phosphate concentration. Further, we demonstrate that a previously published calibration of *D. dianthus* P/Ca is valid in concept but incorrect quantitatively (~10 times lower slope in our new results), while corals growing at $\Omega_{arag} < 1$ have unusually low P/Ca relative to the main calibration regression. We also establish linear relationships for *D. dianthus* between Ba/Ca and dissolved barium concentration, and U/Ca and carbonate ion concentrations. These proxy calibrations do not display primary or secondary residual dependence on temperature, salinity, or pressure. Additionally, P/Ca and Ba/Ca proxies appear to be insensitive to carbonate ion and pH variations.

We propose the use of P/Ca and Ba/Ca in *D. dianthus* as complementary nutrient proxies. Whereas phosphate is regenerated mainly at thermocline depths, dissolved barium profiles resemble those of silicate and alkalinity (Chan et al., 1977; Ostlund et al., 1987) as particulate Ba is regenerated deeper in the water column (Bishop, 1988). As tracers of water mass reorganizations in the past, reconstructed Ba concentrations would be more sensitive to shifts in the biogeochemical structure of deepwater, where the phosphate profile is relatively invariant, and phosphate would have more sensitivity to changes in the structure of thermocline and intermediate waters.

A carbonate ion proxy, measured in a regional set of depth-age distributed *D. dianthus* skeletons, would allow direct reconstruction of lysocline depth in the water column, which when combined with other proxies could provide clues to the importance of atmospheric CO_2, weathering, organic matter rain rate and burial, and carbonate dissolution on the relative position of carbonate saturation horizon and carbonate compensation depth (Archer and Maier-Reimer, 1994; Sigman et al., 1998).

The P/Ca, Ba/Ca, and U/Ca calibrations could be used simultaneously with ^{14}C and U–Th dating to derive ventilation rates in the past from the mixing ratio of distinct endmember water masses in regions with active mixing of intermediate and deepwater sources, like the Atlantic and Southern Oceans. Reconstruction of nutrient abundances and carbonate ion distributions in regions where deep advection is sluggish and nutrient regeneration is relatively more important, like the deep North Pacific, could provide clues about basin-scale variations in export production, changes in whole-ocean nutrient inventory, and shifts in carbonate system equilibria on geological timescales.

The calibrations reported here are based on a globally distributed set of corals, and the scatter around the linear relationships suggests caution in using these calibrations for regional paleo-applications. Given the uncertainties in the calibration regressions of these proposed proxies, seawater phosphate can be reconstructed to ±0.4 μmol/kg (from 1.3 to 1.9 μmol/kg P_{sw}), and seawater Ba to ±19 nmol/kg (from 41 to 82 nmol/kg Ba_{sw}). Carbonate ion concentration derived from U/Ca has an uncertainty of ±31 μmol/kg (from 60 to 120 μmol/kg CO_3^{2-}). The calibrations presented here provide a proof of concept and support the fundamental dependencies of the P/Ca, Ba/Ca and U/Ca proxies in *D. dianthus* on important biogeochemical variables for which paleo-records are currently sparse or controversial.

ACKNOWLEDGMENTS

We thank Liz Sikes (Rutgers University) and Stephen Cairns (Smithsonian Institute) for providing corals for this work. Also we are indebted to Yair Rosenthal for extensive advice and Paolo Montagna for thoughtful discussions. We thank Associate Editor Anne Cohen and the anonymous reviewers for their significant help in improving this manuscript. This work was supported by Grants to RMS from NSF Chemical Oceanography (OCE 0752544) and Marine Geology and Geophysics (OCE 0962260).

APPENDIX

Table A1
Summary of information on coral location, coral chemical properties, and hydrographic parameters at each coral specimen location.

Coral ID	Coral depth (m)	Date coral collection	Coral Lat (N)	Coral Long (W)	Coral data				Dissolved Ba data						
					P/Ca (±1SD) (μmol/mol)	Ba/Ca (±1SD) (μmol/mol)	U/Ca (±1SD) (μmol/mol)	Number of averaged lines (replicate ablations)	GEOSECS Sta (1972–1978) and other stations*		Lat	Long	Depth Hydrographic data (m)	Ba_{sw} (nmol/kg)	References
80358	358	1967	48	8	27.40	5.64 (0.03)	0.85 (0.01)	1 (1) for P/Ca, 1 (3) for rest		23	60	17	400	44	Chan et al. (1977)
48739	825	1973	48	7	63.37 (2.52)	6.29 (0.08)	1.64 (0.03)	1 (4)		23	60	17	886	47	Chan et al. (1977)
48473	1115–1100	1973	48	8	26.69 (2.22)	6.43 (0.34)	0.78 (0.05)	1 (4)		23	60	17	1095	47	Chan et al. (1977)
48740	1470	1973	49	11	55.38 (2.18)	12.12 (0.17)	1.13 (0.07)	1 (3)	Sta. 115 following 27.9 isopycnal from A24 WOCE		28	26	1733	56	Ostlund et al. (1987)
47407	549	1964	−55	130	114.46 (8.34)	10.40 (0.68)	0.93 (0.10)	3 (4) for Ba/Ca, 2 (4) for P/Ca, U/Ca	Sta. 322 following 27.1 σ_t, from P17E WOCE interpolating missing Ba		−43	130	804	54	Ostlund et al. (1987)
47409	686–659	1966	−54	39	75.93 (6.70)	10.12 (0.10)	2.13 (0.08)	1 (3)		74	−55	50	730	83	Chan et al. (1977)
84820	806	1986	0	92	47.75 (2.80)	12.58 (0.40)	2.01 (0.15)	2 (1)	331 along 27.5 σ_t		−5	125	1168	100	Ostlund et al. (1987)
19249	274	1889	34	120	117.57 (7.46)	7.87 (0.52)	2.04 (0.14)	1 (3) and 1 (4)	204 along 26.5 σ_t, interpolating missing Ba (201 closest Sta.)		31	150	415	48	Ostlund et al. (1987)
62309	613–430	1979	40	68	37.71 (10.13)	7.30 (0.27)	1.32 (0.08)	3 (3)		29	36	47	503	43	Chan et al. (1977)
83583	488–440	1986	33	128	81.34	11.71	2.33	1 (1)	26.9 σ_t to station 204 (201 closest Sta.)		31	150	624	68	Ostlund et al. (1987)
47413	421	1964	−51	−168	78.29	8.92	1.79	1 (1)		24*	−49	−145	400	48	Jacquet et al. (2004)
84818	430–373	1986	0	90	64.69 (0.53)	18.65 (0.23)	3.00 (0.09)	1 (3)							
94069	710	1993	−31	179	61.30 (2.53)	7.69 (0.18)	1.76 (0.07)	2 (3)	263 following 27 σ_t from the closest 275 Sta.		−16	167	588	52	Ostlund et al. (1987)
47408	713		−49	−165	97.38 (8.19)	8.77 (0.30)	1.46 (0.05)	1 (4)							
80207	910–915	1967	−47	−148	105.16 (59.34)	11.25 (0.52)	1.35 (0.38)	2 (3)		33*	−51	−143	902	69	Jacquet et al. (2004)
19168	636	1888	−52	74	66.15 (4.88)	8.61 (0.05)	1.84 (0.05)	1 (3)		76	−58	66	646	78	Chan et al. (1977)
78630	312	1982	47	131	38.10 (2.91)	7.86 (0.22)	2.00 (0.11)	2 (3)	204 along 26.8 σ_t interpolating missing Ba (from P0l WOCE)		31	150	566	62	Ostlund et al. (1987)
82065	567–604	1964	−55	130	67.85 (2.42)	12.91 (0.01)	1.77 (0.05)	1 (3)		51*	−54	142	600	77	Jacquet et al. (2004)
45669	494–384	1963	−56	66	101.62 (6.99)	8.48 (0.14)	1.43 (0.05)	1 (3)		76	−58	66	496	76	Chan et al. (1977)
Z9725	276	1999	-45	−172	47.91 (1.27)	5.69 (0.27)	1.23 (0.06)	1 (3)		296	−45	−167	276	51	Ostlund et al. (1987)

Table A2
Continued summary from Table A1. Uncertainties in $PO_{4\text{-sw}}$ and CO_3^{2-} are SD of 2–8 nearby hydrographic stations (see text for details).

Coral ID	Coral depth (m)	Date coral collection	Coral Lat (N)	Coral Long (W)	WOCE Sta.	GEOSECS Sta.	Transect name	Date of hydrographic data	Depth Hydrographic data (m)	Lat	Long	Salinity (psu)	Theta (°C)	Oxygen (μmol/kg)	$PO_{4\text{-sw}}$ (±1SD) (μmol/kg)	Alkalinity (μmol/kg)	TC (μmol/kg)	pCO_2 (μatm)	CO_3^{2-} (±1SD) (μmol/kg) CO_2 sys	References
Seawater Parameters, excluding Ba																				
80358	358	1967	48	8	33		A24	1997	354	49	11	36	11	251	0.6 (0.1)	2336	2129		149	Talley, Lynne
48739	825	1973	48	7	32		A24	1997	808	49	12	36	10	196	1.1 (0.0)	2344	2172		126	Talley. Lynne
48473	1115–1100	1973	48	8	32		A24	1997	1109	49	12	36	8	199	1.1 (0.0)	2348	2182		122	Talley, Lynne
48740	1470	1973	49	11	32		A24	1997	1509	49	12	35	5	243	1.2 (0.0)	2324	2169		112	Talley, Lynne
47407	549	1964	−55	130	141		P17E	1992	563	−54	126	34	6	275	1.6 (0.5)		2127	375	113	Swift, James
47409	686–659	1966	−54	39	19		A16S	2005	651	−53	36	35	2	183	2.2 (0.0)	2347	2260		76	Wanninkhof, Rik Doney, Scott C.
84820	806	1986	0	92	373		P19C	1993	809	0	86	35	6	50	3.0 (0.1)		2301	1721	30	Talley, Lynne
19249	274	1889	34	120	171		P02	2004	287	30	124	34	8	120	2.0 (0.3)	2264	2196		68 (8)	Swift, James
62309	613–430	1979	40	68	73		A22	1997	500	40	66	35	6	201	1.4 (0.0)	2317	2179		105	Joyce, Terrence M.
83583	488–440	1986	33	128	165		P02	2004	464	30	128	34		42	2.8 (0.1)	2293	2284		44 (1)	Swift, James
47413	421	1964	−51	−168	66		P15S	1996	373	−50	−170	34	6	277	1.5 (0.2)	2284	2124		117	Bullister, John L.
84818	430–373	1986	0	90	373		P19C	1993	387	0	86	35	10	12	2.7 (0.1)		2271	1717	36	Talley, Lynne
94069	710	1993	−31	179	191		P06W	2003	700	−31	−177	34	7	211	1.6 (0.2)	2284	2146		104	Fukasawa, Masao
47408	713		−49	−165	27		P11A	1993	797	−49	−155	34	6	198	1.9 (0.2)		2150			Rintoul, Stephen R.
80207	910–915	1967	−47	−148	23		P11A	1993	1058	−47	−155	34	4	196	2.2 (0.2)					Rintoul, Stephen R.
19168	636	1888	−52	74	260		P19C	1993	680	−52	88	34	5	249	1.9 (0.1)		2156	437	97 (1)	Talley, Lynne
78630	312	1982	47	131	12 for carbonate params and 105 for rest		P15N for carbonate params and P01 for rest	1994 for P15N and 1985 for P01	336 (295 for carbonate parameters)	Sta. 12: 50 Sta. 105: 47	Sta. 12: 165 Sta. 105: 131	34	5	115	2.4 (0.1)	2326	2325		42 (5)	Garrett, John F. (P15N) Talley, Lynne (P01)
82065	567–604	1964	−55	130	136 for carbonate params and 134 for rest		P17E	1992	560 (599 for carbonate parameters)	−53	Sta. 134: 130 Sta. 136: 128	34	7	274	1.4 (0.6)		2144	410	112	Swift, James
45669	494–384	1963	−56	66		76		1972–1973		−58	66	34	2	214	2.3 (0.5)					Ostlund et al. (1987)
Z9725	276	1999	−45	−172	77		P15S	1996	265 (330 for carbonate parameters)	−46	172	35	9	245	1.2 (0.1)	2288	2130		117	Bullister, John L.

REFERENCES

Adkins J. F., Boyle E. A., Curry W. B. and Lutringer A. (2003) Stable isotopes in deep-sea corals and a new mechanism for "vital effects". *Geochim. Cosmochim. Acta* **67**, 1129–1143.

Adkins J. F., Cheng H., Boyle E. A., Druffell E. R. M. and Edwards R. L. (1998) Deep-sea coral evidence for rapid change in ventilation of the deep North Atlantic 15, 400 years ago. *Science* **280**, 725–728.

Adkins J. F., Henderson G. M., Wang S.-L., O'Shea S. and Mokadem F. (2004) Growth rates of the deep-sea scleractinia *Desmophyllum cristagalli* and *Enallopsammia rostrata*. *Earth Plan. Sci. Lett.* **227**, 481–490.

Al-Horani F. A., Al-Moghrabi S. M. and de Beer D. (2003) The mechanisms of calcification and its relation to photosynthesis and respiration in the scleractinian coral *Galaxea fascicularis*. *Mar. Biol. Berlin* **142**, 419–426.

Alibert C. and Kinsley L. (2008) A 170-year Sr/Ca and Ba/Ca coral record from the western Pacific warm pool: 2. A window into variability of the New Ireland coastal undercurrent. *J. Geophys. Res.* **113**, C06006, doi: 06010.01029/02007JC004263.

Altabet M. A. and Curry W. B. (1989) Testing models of past ocean chemistry using foraminifera $^{15}N/^{14}N$. *Global Biogeochem. Cycles* **3**, 107–119.

Anagnostou E. and Sherrell R. M. (2008) MAGIC method for subnanomolar orthophosphate determination in freshwater. *Limnol. Oceanogr.: Methods* **6**, 64–74.

Archer D. and Maier-Reimer E. (1994) Effect of deep-sea sedimentary calcite preservation on atmospheric CO_2 concentration. *Nature* **367**, 260–263.

Barnett M. O., Jardine P. M., Brooks S. C. and Selim H. M. (2000) Adsorption and transport of uranium(VI) in subsurface media. *Soil Sci. Soc. Am. J.* **64**, 908–917.

Bevington P. R. and Robinson K. D. (1992) *Data Reduction and Error Analysis for the Physical Sciences*. McGraw-Hill Companies, New York.

Bishop J. K. B. (1988) The barite–opal–organic carbon association in oceanic particulate matter. *Nature* **332**, 341–343.

Bryan W. B. and Hill D. (1941) Spherulitic crystallization as a mechanism of skeletal growth in the hexacorals. *Proc. Royal Soc. Queensland* **52**, 78–91.

Cairns, S. D. (1994) Scleractinia of the temperate North Pacific. *Smiths. Contrib. Zool.* **557**.

Chan L. H., Drummond D., Edmond J. M. and Grant B. (1977) On the barium data from the Atlantic GEOSECS expedition. *Deep Sea Res.* **24**, 613–649.

Cheng H., Adkins J. F., Edwards R. L. and Boyle E. A. (2000) U–Th dating of deep-sea corals. *Geochim. Cosmochim. Acta* **64**, 2401–2416.

Chung G. S. and Swart P. K. (1990) The concentration of uranium in freshwater vadose and phreatic cements in a Holocene ooid cay; a method of identifying ancient water tables. *J. Sedim. Res.* **60**, 735–746.

Cohen A. L., Layne G. D. and Hart S. R. (2001) Kinetic control of skeletal Sr/Ca in a symbiotoic coral: Implications for the paleotemperature proxy. *Paleoceanography* **16**, 20–26. doi:10.1029/1999PA000478.

Cohen A. L. and McConnaughey T. A. (2003) Geochemical perspectives on coral mineralization. In *Biomineralization* (eds. P. M. Dove, J. J. De Yoreo and S. Weiner). Mineralogical Society of America, pp. 151–187.

Cohen A. L., McCorkle D. C., de Putron S., Gaetani G. A. and Rose K. A. (2009) Morphological and compositional changes in the skeletons of new coral recruits reared in acidified seawater: Insights into the biomineralization response to ocean acidification. *Geochem. Geophys. Geosyst.* **10**, Q07005, doi: 10.1029/2009GC002411.

Constantz B. R. (1986) Coral skeleton construction; a physiochemically dominated process. *Palaios* **1**, 152–157.

Cuif J. P. and Dauphin Y. (2004) The environment recording unit in coral skeletons: structural and chemical evidences of a biochemically driven stepping-growth process in coral fibres. *Biogeosci. Discuss* **1**, 625–658.

Cuif J.-P., Dauphin Y., Doucet J., Salome M. and Susini J. (2003) XANES mapping of organic sulfate in three scleractinian coral skeletons. *Geochim. Cosmochim. Acta* **67**, 75–83.

Cusack M., England J., Dalbeck P., Tudhope A., Fallick A. and Allison N. (2008) Electron backscatter diffraction (EBSD) as a tool for detection of coral diagenesis. *Coral Reefs* **27**, 905–911.

De Villiers J. P. R. (1971) Crystal structures of aragontie, strontianite, and witherite. *Am. Mineralogist* **56**, 758–766.

Dickson A. G. and Millero F. J. (1987) A comparison of the equilibrium constants for the dissociation of carbonic acid in seawater media. *Deep Sea Res. I* **34**, 1733–1743.

Dietzel M., Gussone N. and Eisenhauer A. (2004) Co-precipitation of Sr^{2+} and Ba^{2+} with aragonite by membrane diffusion of CO_2 between 10 and 50 °C. *Chem. Geol.* **203**, 139–151.

Dodge R., Jickells T., Knap A., Boyd S. and Bak R. (1984) Reef-building coral skeletons as chemical pollution (phosphorus) indicators. *Mar. Pollut. Bull.* **15**, 178–187.

Eggins S. M. (2003) Laser ablation ICP–MS analysis of geological materials prepared as lithium borate glasses. *Geostand. Newslett.* **27**, 147–162.

Eggins S. M., Kinsley L. P. J. and Shelley J. M. G. (1998) Deposition and element fractionation processes during atmospheric pressure laser sampling for analysis by ICP–MS. *Appl. Surf. Sci.* **127–129**, 278–286.

Eggins S. M. and Shelley J. M. G. (2002) Compositional heterogeneity in NIST SRM 610-617 glasses. *Geostand. Newslett.* **26**, 269–286.

Farré B., Cuif J.-P. and Dauphin Y. (2010) Occurrence and diversity of lipids in modern coral skeletons. *Zoology* **113**, 250–257.

Feely R. A., Gendron J. F., Baker E. T. and Lebon G. T. (1994) Hydrothermal plumes along the East Pacific Rise, 8° 40' to 11° 50′N: particle distribution and composition. *Earth Planet. Sci. Lett.* **128**, 19–36.

Gaetani G. A. and Cohen A. L. (2006) Element partitioning during precipitation of aragonite from seawater: a framework for understanding paleoproxies. *Geochim. Cosmochim. Acta* **70**, 4617–4634.

Gagnon A. C., Adkins J. F., Fernandez D. P. and Robinson L. F. (2007) Sr/Ca and Mg/Ca vital effects correlated with skeletal architecture in a scleractinian deep-sea coral and the role of Rayleigh fractionation. *Earth Plan. Sci. Lett.* **261**, 280–295.

Goreau T. F., Goreau N. I. and Yonge C. M. (1971) Reef corals: Autotrophs or heterotrophs? *Biol. Bull.* **141**, 247–260.

Guillong M., Horn I. and Günther D. (2003) A comparison of 266 nm, 213 nm and 193 nm produced from a single solid state Nd:YAG laser for laser ablation ICP–MS. *J. Anal. Atom. Spec.* **18**, 1224–1230.

Günther D., Horn I. and Hattendorf B. (2000) Recent trends and developments in laser ablation-ICP-mass spectrometry. *Fresenius J. Anal. Chem.* **368**, 4–14.

Hathorne E. C., Alard O., James R. H. and Rogers N. W. (2003) Determination of intratest variability of trace elements in foraminifera by laser ablation inductively coupled plasma-mass spectrometry. *Geochem. Geophys. Geosyst.* **4**, 8408. doi:10.1029/2003GC000539.

Hathorne E. C., James R. H., Savage P. and Alard O. (2008) Physical and chemical characteristics of particles produced by

laser ablation of biogenic calcium carbonate. *J. Anal. Atom. Spec.* **23**, 240–243.

Hendy E. J., Gagan M. K., Lough J. M., McCulloch M. and deMenocal P. B. (2007) Impact of skeletal dissolution and secondary aragonite on trace element and isotopic climate proxies in Porites corals. *Paleoceanography* **22**, PA4101. doi:10.1029/2007PA001462.

Holcomb M., Cohen A. L., Gabitov R. I. and Hutter J. L. (2009) Compositional and morphological features of aragonite precipitated experimentally from seawater and biogenically by corals. *Geochim. Cosmochim. Acta* **73**, 4166–4179.

Isa Y. and Okazaki M. (1987) Some observations on the Ca^{2+} -binding phospholipid from scleractinian coral skeletons. *Comp. Biochem. Physiol.* **87B**, 507–512.

Jacquet S. H. M., Dehairs F. and Rintoul S. (2004) A high resolution transect of dissolved barium in the Southern Ocean. *Geophys. Res. Lett.* **31**, L14301. doi:10.1029/2004GL020016.

Jochum K. P., Nohl U., Herwig K., Lammel E., Stoll B. and Hofmann A. W. (2005) GeoReM: a new geochemical database for reference materials and isotopic standards. *Geostand. Geoanal. Res.* **29**, 333–338.

Keigwin L. D. and Boyle E. A. (1989) Late Quaternary paleochemistry of high-latitude surface waters. *Palaeogeogr. Palaeoclim. Palaeoec.* **73**, 85–106.

Kitano Y. and Oomori T. (1971) The coprecipitation of uranium with calcium carbonate. *J. Ocean. Soc. Jpn.* **27**, 34–42.

Kleypas J. A., Buddemeier R. W., Archer D., Gattuso J.-P., Langdon C. and Opdyke B. N. (1999) Geochemical consequences of increased atmospheric carbon dioxide on coral reefs. *Science* **284**, 118–120.

Konhauser K. O. (1997) Bacterial iron biomineralisation in nature. *FEMS Microb. Rev.* **20**, 315–326.

Koroleff F. (1983) Determination of nutrients. In *Methods of Seawater Analysis* (eds. M. Ehrhardt and K. Grasshoff). Verlag Chemie, pp. 125–132.

Langdon C., Takahashi T., Sweeney C., Chipman D., Goddard J., Marubini F., Aceves H., Barnett H. and Atkinson M. J. (2000) Effect of calcium carbonate saturation state on the calcification rate of an experimental coral reef. *Global Biogeochem. Cycles* **14**, 639–654.

Langmuir D. (1978) Uranium mineral-solution equilibria. *Geochim. Cosmochim. Acta* **42**, 547–569.

LaVigne M., Field M. P., Anagnostou E., Grottli A. G., Wellington G. M. and Sherrell R. M. (2008) Skeletal P/Ca tracks upwelling in Gulf of Panamá coral: evidence for a new seawater phosphorus proxy. *Geophys. Res. Lett.* **35**, L05604. doi:10.1029/2007GL031926.

LaVigne M., Matthews K. A., Grottoli A. G., Cobb K. M., Anagnostou E., Cabioch G. and Sherrell R. M. (2010) The coral skeleton P/Ca proxy: multi-colony calibration with a contemporaneous seawater phosphate record and potential for global application. *Geochim. Cosmochim. Acta* **74**, 1282–1293.

Lazier A. V., Smith J. E., Risk M. J. and Schwarcz H. P. (1999) The skeletal structure of *Desmophyllum cristagalli*: the use of deep-water corals in sclerochronology. *Lethaia* **32**, 119–130.

Lea D. W. and Boyle E. A. (1990) Foraminiferal reconstruction of barium distributions in water masses of the glacial oceans. *Paleoceanography* **5**, 719–742.

Lea D. W., Shen G. T. and Boyle E. A. (1989) Coralline barium records temporal variability in equatorial Pacific upwelling. *Nature* **340**, 373–375.

Lewis E. and Wallace D. W. R. (1998) *Program Developed for CO_2 System Calculations*. ORNL/CDIAC-105. Carbon Dioxide Information Analysis Center, Oak Ridge National Laboratory, US Department of Energy, Oak Ridge, TN.

Longerich H. P., Günther D. and Jackson S. E. (1996a) Elemental fractionation in laser ablation inductively coupled plasma mass spectrometry. *Fresenius J. Anal. Chem.* **355**, 538–542.

Longerich H. P., Jackson S. E. and Günther D. (1996b) Laser ablation inductively coupled plasma mass spectrometric transient signal data acquisition and analyte concentration calculation. *J. Anal. Atom. Spec.* **11**, 899–904.

Macintyre I. G., Bayer F. M., Logan M. A. V. and Skinner H. C. W. (2000) Possible vestige of early phosphatic biomineralization in gorgonian octocorals (Coelenterata). *Geology* **28**, 455–458.

Marchitto T. M., Lynch-Stieglitz J. and Hemming S. R. (2005) Deep Pacific $CaCO_3$ compensation and glacial-interglacial atmospheric CO_2. *Earth Plan. Sci. Lett.* **231**, 317–336.

McCorkle D. C., Martin P. A., Lea D. W. and Klinkhammer G. P. (1995) Evidence of a dissolution effect on benthic foraminiferal shell chemistry: $\delta^{13}C$, Cd/Ca, Ba/Ca, and Sr/Ca results from the Ontong Java Plateau. *Paleoceanography* **10**, 699–714.

Mehrbach C., Culberson C. H., Hawley J. E. and Pytkowicz R. M. (1973) Measurement of the apparent dissociation constants of carbonic acid in seawater at atmospheric pressure. *Limnol. Oceanogr.* **18**, 897–907.

Meibom A., Yurimoto H., Cuif J. P., Domart-Coulon I., Houlbreque F., Constantz B., Dauphin Y., Tambutté E., Tambutté S., Allemand D., Wooden J. and Dunbar R. (2006) Vital effects in coral skeleton composition display strict three-dimensional control. *Geophys. Res. Lett.* **33**, L11608. doi:10.1029/2006GL025968.

Min G. R., Edwards L. R., Taylor F. W., Recy J., Gallup C. D. and Beck W. J. (1995) Annual cycles of U/Ca in coral skeletons and U/Ca thermometry. *Geochim. Cosmochim. Acta* **59**, 2025–2042.

Montagna P., McCulloch M., Taviani M., Mazzoli C. and Vendrell B. (2006) Phosphorus in cold-water corals as a proxy for seawater nutrient chemistry. *Science* **312**, 1788–1791.

Nothdurft L. D., Webb G. E., Brostrom T. and Rintoul L. (2007) Calcite-filled boring in the most recently deposited skeleton in live-collected Porites (Scleractinia): Implications for trace element archives. *Geochim. Cosmochim. Acta* **71**, 5423–5438.

Ogilvie M. M. (1896) Microscopic and systematic study of madreporarian types of corals. *Phil. Trans. B* **187**, 83–345.

Ostlund H. G., Craig H., Broecker W. S. and Spencer D. (1987) *Atlantic, Pacific, and Indian Ocean Expeditions, Shorebased Data and Graphics*. International Decade of Ocean Exploration, NSF, Washington, DC.

Pena L. D., Cacho I., Calvo E., Pelejero C., Eggins S. and Sadekov A. (2008) Characterization of contaminant phases in foraminifera carbonates by electron microprobe mapping. *Geochem. Geophys. Geosys.* **9**, Q07012. doi:10.1029/2008GC002018.

Pena L. D., Calvo E., Cacho I., Eggins S. and Pelejero C. (2005) Identification and removal of Mn–Mg-rich contaminant phases of foraminiferal tests: implications for Mg/Ca past temperature reconstructions. *Geochem. Geophys. Geosys.* **6**, Q09P02. doi:10.1029/2005GC000930.

Perrin C. and Smith D. C. (2007) Decay of skeletal organic matrices and early diagenesis in coral skeletons. *C.R. Palevol.* **6**, 253–260.

Reed W. P. (1992) NIST certificate of analysis. *Stand. Ref. Mater.* **612**, 613.

Reeder R. J., Nugent M., Lamble G. M., Tait C. D. and Morris D. E. (2000) Uranyl incorporation into calcite and aragonite: XAFS and luminescence studies. *Environ. Sci. Technol.* **34**, 638–644.

Reeder R. J., Nugent M., Tait C. D., Morris D. E., Heald S. M., Beck K. M., Hess W. P. and Lanzirotti A. (2001) Coprecipitation of Uranium(VI) with Calcite: XAFS, micro-XAS, and

luminescence characterization. *Geochim. Cosmochim. Acta* **65**, 3491–3503.

Ricker W. E. (1973) Linear regressions in fishery research. *J. Fish. Res. Board Can.* **30**, 409–434.

Ries J., Cohen A. and McCorkle D. (2010) A nonlinear calcification response to CO_2-induced ocean acidification by the coral *Oculina arbuscula*. *Coral Reefs* **29**, 661–674.

Robinson L. F., Adkins J. F., Keigwin L. D., Southon J., Fernandez D. P., Wang S. L. and Scheirer D. S. (2005) Radiocarbon variability in the western North Atlantic during the last deglaciation. *Science* **310**, 1469–1473.

Rosenthal Y., Boyle E. A. and Labeyrie L. (1997) Last glacial maximum paleochemistry and deepwater circulation in the Southern Ocean: evidence from foraminiferal cadmium. *Paleoceanography* **12**, 787–796.

Russell A. D., Hönisch B., Spero H. J. and Lea D. W. (2004) Effects of seawater carbonate ion concentration and temperature on shell U, Mg, and Sr in cultured planktonic foraminifera. *Geochim. Cosmochim. Acta* **68**, 4347–4361.

Schneider K. and Erez J. (2006) The effect of carbonate chemistry on calcification and photosynthesis in the hermatypic coral *Acropora eurystoma*. *Limnol. Oceanogr.* **51**, 1284–1293.

Shen G. T., Boyle E. A. and Lea D. W. (1987) Cadmium in corals as a tracer of historical upwelling and industrial fallout. *Nature* **328**, 794–896.

Shen G. T. and Dunbar R. B. (1995) Environmental controls on uranium in reef corals. *Geochim. Cosmochim. Acta* **59**, 2009–2024.

Sherwood B. A., Sager S. L. and Holland H. D. (1987) Phosphorus in foraminiferal sediments from North Atlantic ridge cores and in pure limestones. *Geochim. Cosmochim. Acta* **51**, 1861–1866.

Shotyk W., Immenhauser-Potthast I. and Vogel H. (1995) Determination of nitrate, phosphate, and organically bound phosphorus in coral skeletons by ion chromatography. *J. Chrom. A* **706**, 209–213.

Sigman D. M., McCorkle D. C. and Martin W. R. (1998) The calcite lysocline as a constraint on glacial/interglacial low-latitude production changes. *Global Biogeochem. Cycles* **12**, 409–427.

Sinclair D. J., Kinsley L. P. J. and McCulloch M. T. (1998) High resolution analysis of trace elements in corals by laser ablation ICP–MS. *Geochim. Cosmochim. Acta* **62**, 1889.

Sinclair D. J., Williams B. and Risk M. (2006) A biological origin for climate signals in corals-Trace element "vital effects" are ubiquitous in Scleractinian coral skeletons. *Geophys. Res. Lett.* **33**, L17707. doi:10.1029/2006GL027183.

Speer J. A. (1983) Crystal chemistry and phase relations of orthorhombic carbonates. In *Carbonates: Mineralogy and Chemistry* (ed. R. J. Reeder), pp. 145–190.

Stanley G. D. and Cairns S. D. (1988) Constructional azooxanthellate coral communities: an overview with implications for the fossil record. *Palaios* **3**, 233–242.

Swart P. K. and Hubbard J. A. E. B. (1982) Uranium in scleractinian coral skeletons. *Coral Reefs* **1**, 13–19.

Tudhope A. W., Lea D. W., Shimmield G. B., Chilcott C. P. and Head S. (1996) Monsoon climate and Arabian Sea coastal upwelling recorded in massive corals from Southern Oman. *Palaios* **11**, 347–361.

Yu J. and Elderfield H. (2007) Benthic foraminiferal B/Ca ratios reflect deep water carbonate saturation state. *Earth Plan. Sci. Lett.* **258**, 73–86.

Associate editor: Anne Cohen